Austin Journal of Radiology

Open Access

Austin Publishing Group

Review Article

Milestone Research on Meniere's Disease by Visualizing Endolymphatic Hydrops Using Gadolinium-Enhanced Inner Ear MRI and the Challenges in Clinical Applications

Zou J[1,2]*, Pyykkö I[1], Yoshida T[3], Gürkov R[4], Shi H[6], Li Y[7], Zheng G[2], Zhao Z[2], Peng R[2], Zheng H[2], Yin S[6],Hyttinen J[8], Nakashima T[3] and Naganawa S[5]

[1]Hearing and Balance Research Unit, Field of Oto-laryngology, School of Medicine, University of Tampere, Finland

[2]Department of Otolaryngology-Head and Neck Surgery, Changhai Hospital, Second Military Medical University, China

[3]Department of Otorhinolaryngology, Nagoya University, Graduate School of Medicine, Japan

[4]Department of Otorhinolaryngology-Head and Neck Surgery, University of Munich, Germany

[5]Department of Radiology, Nagoya University, Graduate School of Medicine, Japan

[6]Department of Otolaryngology-Head & Neck Surgery, Affiliated Sixth People's Hospital of Shanghai Jiao Tong University, China

[7]Department of Radiology, Affiliated Sixth People's Hospital of Shanghai Jiao Tong University, China

[8]Department of Electronics and Communications Engineering and BioMediTech, Tampere University of Technology, Finland

***Corresponding author:** Zou J, Hearing and Balance Research Unit, Field of Oto-laryngology, School of Medicine, University of Tampere, Medisiinarinkatu 3, 33520 Tampere, Finland

Received: August 07, 2015; **Accepted:** September 01, 2015; **Published:** September 04, 2015

Abstract

This review discusses the history of detecting Endolymphatic Hydrops (EH) and collecting evidence to diagnose Meniere's Disease (MD) using Gadolinium-enhanced Inner Ear MRI (Gd-IEMRI) and the challenges in clinical applications. EH was visualized *in vivo* using Gd-IEMRI in an animal model by Zou et al. in 2000 at the Karoliniska Institutet. The perilymphatic and endolymphatic spaces were observed separately in humans using Gd-IEMRI with a 1.5 T machine after transtympanic injection of Gadolinium Chelate (GdC) in 2005 at the University of Tampere. EH in patients with MD was clearly demonstrated by Nakashima et al. with a 3.0 T machine with a 3-Dimensional Fluid-Attenuated Inversion Recovery (3D-FLAIR) sequence in 2007 at Nagoya University. The oval window was shown to be the major pathway for GdC to enter the inner ear after transtympanic injection. Long-term hearing function assessment after intratympanic application of GdC showed no evidence of ototoxicity in patients. The image quality correlated with various coils in addition to the magnetic strength of MRI. Naganawa et al. developed the following sequences to improve sensitivity: 3-Dimensional Fluid-Attenuated Inversion Recovery (3D-FLAIR), Heavily T(2)-weighted (hT(2)W)-3D-FLAIR, subtracting a positive endolymph image from a positive perilymph image that was called HYDROPS (i.e., HYbriD of Reversed image Of Positive endolymph signal and native image of positive perilymph Signal), and the HYDROPS2-Mi2 method (i.e., HYbriD of Reversed image Of MR cisternography and a positive Perilymph Signal by heavily T2-weighted 3DFLAIR-Multiplied by T2). Computer-aided segmentation of endo- and perilymph spaces reduces the observer-dependence of hydrops quantification and allows for volumetric quantification.

Keywords: Meniere's disease; MRI; Endolymphatichydrops; Diagnosis; Contrast agent

Introduction

Endolymphatic Hydrops (EH) is accepted as a typical pathological change in Meniere's Disease (MD),which was independently described by KyoshiroYamakawa (1892-1980) [1] and by Charles Skinner Hallpike (1900-1979) and Hugh Cairns (1896-1952) in 1938 [2]. Traditionally, MD has been considered an idiopathic condition comprising episodic rotatory vertigo, fluctuant hearing loss and tinnitus. It was first described and defined *per se* by Prosper Menière (1799-1862) in his publication in September 1861 [3] and has had his name associated with it largely since that time. Since then, the additional symptoms of aural pressure, hyperacusis and ataxia have come to be associated with the condition. Currently, MD is diagnosed as possible MD, probable MD, definite MD, and certain MD according the guidelines provided by the American Academy of Otolaryngology-Head and Neck Foundation, Inc [4]. A diagnosis of certain MD was once only made after a postmortem histological study. However, this was changed by an MRI study with an animal model by Zou et al. that showed EH *in vivo* after intravenous injection of Gadolinium Chelate (GdC) [5,6]. A high dose of GdC was applied to induce enough distribution in the inner ear because the transport efficacy of GdC across the blood-perilymph barrier is poor, which had the risk of causing renal injury and even nephrogenic systemic fibrosis [7-9]. Thereafter, high contrast images of all cochlear turns were obtained after placing GdC on the round window membrane. Subsequently, the perilymphatic and endolymphatic spaces were first observed separately in humans in 2005 using a 1.5 T machine after transtympanic injection of GdC [10]. Clear visualization of EH in MD patients was first demonstrated in 2007 using a 3.0 T machine with a three-Dimensional Fluid-Attenuated Inversion Recovery (3D-FLAIR) sequence after transtympanic injection of GdC diluted eightfold with saline [11]. This review discusses the development of the technique and challenges during clinical applications.

Animal models of EH

It has been reported that EH might be induced in animals by surgically blocking the endolymphatic duct and sac, inducing immune injury of the endolymphatic sac (challenged with keyhole

Citation: Zou J, Pyykkö I, Yoshida T, Gürkov R, Shi H, Li Y, et al. Milestone Research on Meniere's Disease by Visualizing Endolymphatic Hydrops Using Gadolinium-Enhanced Inner Ear MRI and the Challenges in Clinical Applications. Austin J Radiol. 2015; 2(6): 1035.

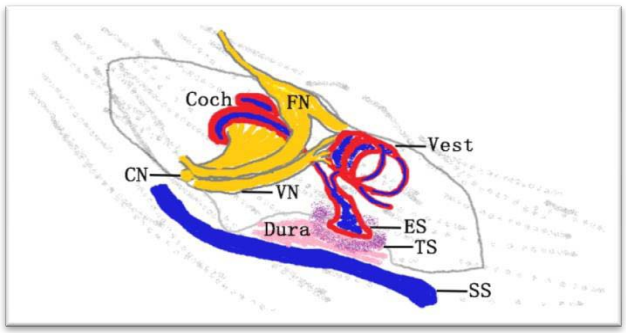

Figure 1: Illustration of Zou's modified surgical model of endolymphatic hydrops in guinea pigs. The Endolymphatic Sac (ES) was isolated from the Sigmoid Sinus (SS) and sealed with Tissue Sealant (TS). Coch: Cochlea; CN: Cochlear Nerve; FN: Facial Nerve; Vest: Vestibule; VN: Vestibular Nerve.

limpet hemocyanin, KLH), and using noise exposure [12-15]. The immune injury and noise exposure models were advantageous to explore the etiology of MD [16-20]. In the early phase following a secondary KLH challenge, hearing thresholds significantly increased simultaneously with the elevation of perilymph antibody levels. The degree of hydrops was not the only factor causing the hearing loss as well as elevated ration of the action potential to the summating potential. Scale-out hearing loss appeared in animals with severe degeneration of the striavascular is as well as the organ of Corti, which was associated with inflammatory cellular infiltration, especially in the perilymphatic space, even in the absence of KLH in the cochlea [14]. The surgical model focused on the target of the endolymphatic sac and was concerned with its function of absorbing endolymph. However, Kimura's model was aggressive because it destroyed the endolymphatic duct and sac [12]. Zou et al. further improved the surgical model by gently dissecting the endolymphatic sac from the sigmoid sinus and covering its outer surface with tissue sealant (Figure 1). The endolymphatic sac was kept intact but was defunctionalized, and EH could be visualized during the acute stage (6 days after operation) with MRI [5,6,21]. Later on, immune injury of the inner ear was induced by challenging the round window with KLH, which mimicked MD secondary to the otitis media, and EH was visualized using MRI [22,23].

Validation of the MRI method in demonstrating EH

The first MRI showing EH in an animal model was actually discovered by accident on February 21, 2000, at the Karoliniska Institute. The primary purpose of the study was to detect leakage of GdC into the cochlear endolymphatic space (i.e., scala media) to indicate a pathological change in the striavascularis, which was observed in impulse noise-induced hearing loss [24]. Anguinea pig with endolymphatic sac damage plus intraperitoneal injection of 1 mg/kg D-aldosterone was imaged using a 4.7 T MRI after intravenous injection of GdC. The appearance of an excellent cochlear MRI was expected with slightly contrasted scala media distinguishable from the highly contrasted scala tympani and vestibuli. However, the images were disappointing in that the expected bright scalavestibuli (as result of taking up GdC) was almost unidentifiable, and the scala media did not show any sign of leakage after taking up the Gdc. The only obvious bright dots were located in the expected area of the scala tympani. After an intensive search for a potential error in the system

Figure 2: The first picture of endolymphatic hydrops in an animal model shown by MRI. NT: Non-Treated side; Op: treated side. SM: Scalamedia; ST: Scala Tympani; SV: Scalavestibuli; 1H: basal Higher turn; 2L: Second Lower turn; 2H: Second Higher turn; 3L: Third Lower turn; 3H: Third Higher turns. Scale bar = 1 mm.

Table 1: Signal intensities in the scala tympani of a guinea pig in gadolinium-enhanced MRI acquired using a 4.7 T machine at 50 days after endolymphatic sac damage plus intraperitoneal injection of D-aldosterone.

Location	Signal intensity (arbitrary unit)*	
	operated ear	non-treated ear
1L	69.7	69.8
1H	76.8	81.2
2L	86.4	66.8
2H	103.0	72.1
3	79.1	57.4

*Signal intensities in the region of interest were analyzed using ImageJ v1.46r (National Institute of Health, Bethesda, USA). Cochlear action potential threshold measured by electrocochleography was 65 dB SLP in the treated ear and 25 in the non-treated ear. 1H: the first higher turn; 2L: the second lower turn, etc.; 3: the third turn including the lower and higher parts.

that resulted in poor quality of the images, it was realized that the cause of the poor images in the gadolinium-enhanced MRI was severe EH [5,6]. The unidentifiable scalavestibuli was the result of EH in the scala media that occupied the majority of the area of the scalavestibuli (Figure 2). The signal intensities in the scala tympani of the second and third turns of the treated side were higher than that of the non-treated side (Table 1), which was not reported previously.

The accuracy of MRI in detecting EH was confirmed by histological study in the animal model using agar embedding. The degree of EH shown by MRI correlated very well with that demonstrated by histology [6].

Intratympanic delivery of GdC

High-dose GdC has been applied to induce adequate distribution in the inner ear in order to overcome poor transport efficacy of GdC across the blood-perilymph barrier, which has a risk of causing renal injury and even nephrogenic systemic fibrosis [7-9]. Therefore, intratympanic administration of GdC was tested in guinea pigs by placing the contrast agent on the round window membrane and inducing high contrast images of all four cochlear turns that were achieved using a 4.7 T experimental MRI [25]. Subsequently, a clinically feasible method of transtympanic injection of GdC was applied, and the perilymphatic and endolymphatic spaces were observed separately in humans using a 1.5 T clinical MRI [10]. In order to further reduce the amount of contrast agent applied to the body, a targeted delivery of GdC to the tympanic medial wall was developed in a minimally invasive way, and this generated efficient

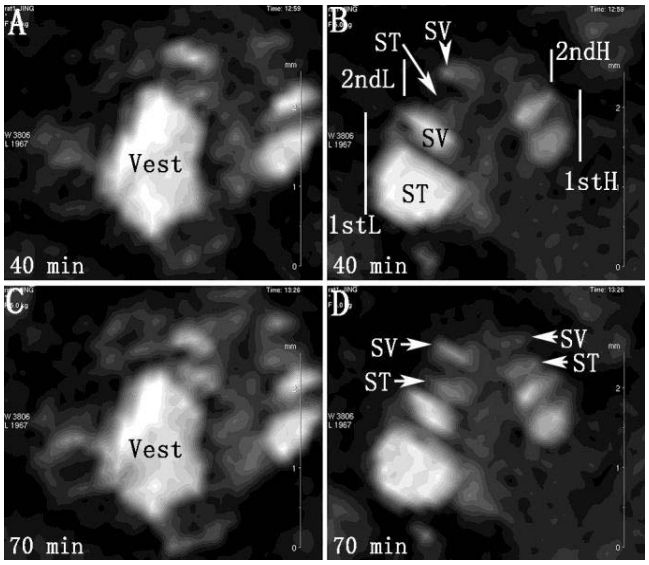

Figure 3: Distribution of Gd-DOTA in the rat inner ear after targeted delivery to the tympanic medial wall shown by MRI. A 2.5 µl volume of 0.5 M Gd-DOTA was injected through a high-performance polyimide tube. At 40 min post-administration, the Vestibule (Vest) demonstrated sufficient uptake of Gd-DOTA (A). Significantly higher signal intensity in the Scalavestibuli (SV) than that in the Scala Tympani (ST) of the Second Lower turn (2ndL) suggests that Gd-DOTA in the SV was directly transported from the oval window through vestibule instead of the round window through the ST (B). At 70 min after delivery, there was insignificant signal change in the vestibule (C) and significant increase in the Gd-DOTA uptake in higher coils of the cochlea (D). 1stL: basal lower turn; 1stH: basal higher turn; 2ndH: Second Higher turn.

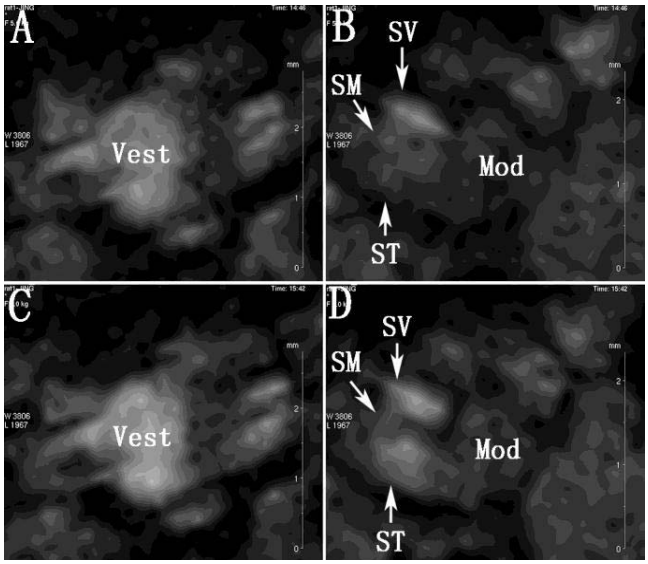

Figure 4: Distribution of Mn^{++} in the rat inner ear after targeted delivery to the tympanic medial wall shown by MRI. A 4 µl volume of 0.5 M $MnCl_2$ was injected through a high-performance polyimide tube. At 100 min post-administration, there was abundant uptake of Mn^{++} in the Vestibule (Vest) (A) and significantly greater distribution in the Scalavestibuli (SV) than Scala Tympani (ST) in the cochlea (B). At 160 min after delivery, there was a slight increase inMn^{++} in the vestibule (C), and the intensity of Mn^{++} became close between the scalavestibuli and scala tympani (D).

uptake of GdC in the inner ear of rats [26]. The minimally invasive and targeted delivery method was shown to be efficient enough to highlight the inner ear perilymphatic spaces and demonstrate EH in patients with a 3 T MRI [27]. The transport passages from the middle ear to the inner ear were shown to be through both the oval and round windows, and the previous one was more efficient than the later (Figure 3) [28]. The oval window passage was facilitated in the perilymphatic fistula and was reduced in MD with severe EH [29,30].

Auditory brainstem response measurements showed no significant threshold shifts after round window application of GdC, indicating that the contrast agent was non-toxic to the guinea pig cochlea [25]. Transtympanic injection of non-diluted Gadolinium Hydrate (GdH) decreased the endocochlear potential and enlarged the intercellular spaces in the striavascular is, which did not occur in the guinea pigs that received transtympanic injection of GdH diluted eightfold with saline (1/8 GdH) [31]. The clinically applied GdC must be safer than the GdH in the inner ear after transtympanic injection. Both short- and long-term hearing function assessments after intratympanic application of gadolinium-based agent showed no evidence of ototoxicity in patients with definite MD and in patients with possible MD, and normal auditory thresholds were maintained [32,33].

Intratympanic delivery of manganese ion

Pautler et al. first reported that Manganese-Enhanced MRI (MEMRI) was capable of tracking neuronal connections *in vivo* in the nose and eyes of mice after topical administration [34]. The underlying mechanism was that the Mn^{++} acts as a functional Ca^{++} analog in addition to its T1 contrast effect. Mn^{++} has an ionic radius similar to that of Ca^{++} and is handled similarly in many biological systems [35]. Similarly, Mn^{++} ions enter excitable cells through voltage-gated calcium channels and can become sequestered in mitochondria and secretory granules [36-38]. Therefore, MEMRI was used to trace the central auditory pathway in living animals after either topical or systemic administration [38-40]. MEMRI has been used to follow neural activity in the brain, including regions of accumulated sound-evoked activity in normal animals, tinnitus-related brain regions, noise-induced activity increases in the brain, and central neuroplasticity (including hyperactivity) and neurodegenerative mechanisms associated with age-related hearing loss [41-44]. Recently, alterations in calcium transport (possibly due to Ca^{++}-ATPase dysfunction) in preclinical models of cardiac hypertrophy were visualized using MEMRI [45]. That report broadened the application of MEMRI from detecting neuronal activity to monitoring Ca^{++} homeostatic maintenance. Consequently, the detection of Ca^{++} transport in the inner ear *in vivo* using MEMRI after minimally invasive and targeted administration of Mn^{++} (2.5 µl $MnCl_2$ solution, 500 mM) to the tympanic medial wall was reported in rats (Figure 4) [46].

Development of MRI sequences for clinical applications

In 2007, Nakashima et al. reported clear visualization of EH in MD patients using a 3.0 T machine with a three-Dimensional Fluid-Attenuated Inversion Recovery (3D-FLAIR) sequence by differentiating the endolymphatic space from the perilymphatic space after transtympanic injection of GdC diluted eightfold with saline [11]. However, 3D-FLAIR was unable to differentiate the endolymphatic space from the surrounding bone. In 2008, Naganawa et al. reported a 3D Inversion-Recovery Turbo Spin Echo (3D-IR TSE) with real

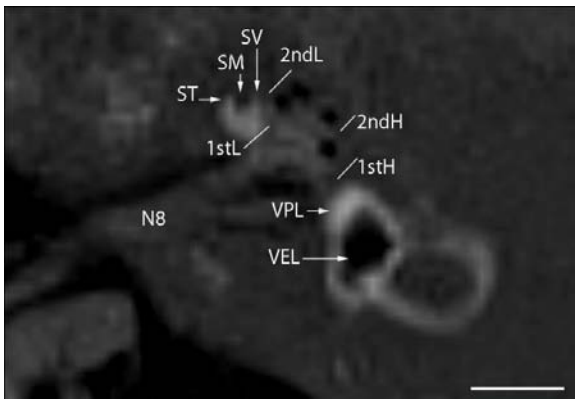

Figure 5: Separate visualization of endolymphatic and perilymphatic spaces and bone in human using 3D real IR TSE on 3 T MRI after intratympanic administration of Gd-DTPA. A 48-year-old man with left Meniere's disease. Images were obtained 24 h after transtympanic injection of 50 mMGd-DTPA at 3T using a 32 channel head coil. N8: 8th cranial Nerve; SM: Scala Media; ST: Scala Tympani; SV: Scalavestibuli; VEL: Vestibular Endolymph; VPL: Vestibular Perilymph; 1stL: basal Lower turn; 1stH: basal Higher turn; 2ndL: Second Lower turn; 2ndH: Second Higher turn. Scale bar = 5 mm.

reconstruction that separated the signals of the perilymphatic space (positive value), endolymphatic space (negative value) and bone (near zero) by setting the inversion time between the null point of Gd-containing perilymph fluid and that of the endolymph fluid without Gd (Figure 5) [47].

The original method of inner ear MRI post-intravenous injection of GdC was capable of detecting permeability changes in the blood-inner ear barrier that was missing in the approach of intratympanic delivery of GdC [5,6,10, 25]. It is clinically valuable to develop a sensitive MRI method for detecting weak Gd signals in the perilymph after intravenous injection of single-dose GdC. Naganawa et al. demonstrated that heavily T(2)-weighted (hT(2)W)-3D-FLAIR was capable of detecting the Gd signal in the perilymph of MD patients using a 32-channel coil after intravenous injection of a single dose of GdC [48-50]. This method first enabled clear visualization and evaluation of EH in MD patients with a clinically feasible method. The same group further improved the image quality by subtracting a positive endolymph image from a positive perilymph image, which was called HYDROPS (i.e., HYbriD of Reversed image Of Positive endolymph signal and native image of positive perilymph Signal), in which the T1 relaxivity of Gadolinium-Diethylenetriamine Pentaacetate-Bismet-Bismethylamide (Gd-DTPA-BMA) was taken into account to highlight the endolymph and perilymph separately [51].

However, the imaging time was long (over 30 min using a Tim 4G Head/Neck 20 coil), which is impractical in hospitals, especially in China. A HYDROPS2-Mi2 method (i.e., HYbriD of Reversed image Of MR cisternography and a positive Perilymph Signal by heavily T2-weighted 3D-FLAIR-Multiplied by T2) was further developed in which the imaging time was reduced by two-thirds (Figure 6) [52]. However, the HYDROPS2-Mi2 method needs validation with more details.

Recently, volumetric quantification of EH was reported to be more precise and less related to human judgment than previous methods (Figure 7). This method employed the advantage of a heavily

Figure 6: Comparing the detection of Gd-uptake in the inner ear of MD patients using the methods of HYDROPS-Mi2 and HYDROPS2-Mi2. A 50-year-old man with right Meniere's disease. Images were obtained 4 hours after single dose intravenous GdC administration at 3T using a 32 channel head coil. Image A is HYDROPS-Mi2 obtained in 31 minutes of scan time. Image B is HYDROPS2-Mi2 obtained in 17 minutes. Image C is HYDROPS2-Mi2 obtained in 10 minutes. Although the cochlear endolymph space seems to be slightly larger on HYDROPS-Mi2, the vestibular endolymph space seems to be similar among the3 images. N8: 8th cranial Nerve; SM: Scala Media; ST: Scala Tympani; VEL: Vestibular Endolymph; VPL: Vestibular Perilymph. Scale bar = 5 mm.

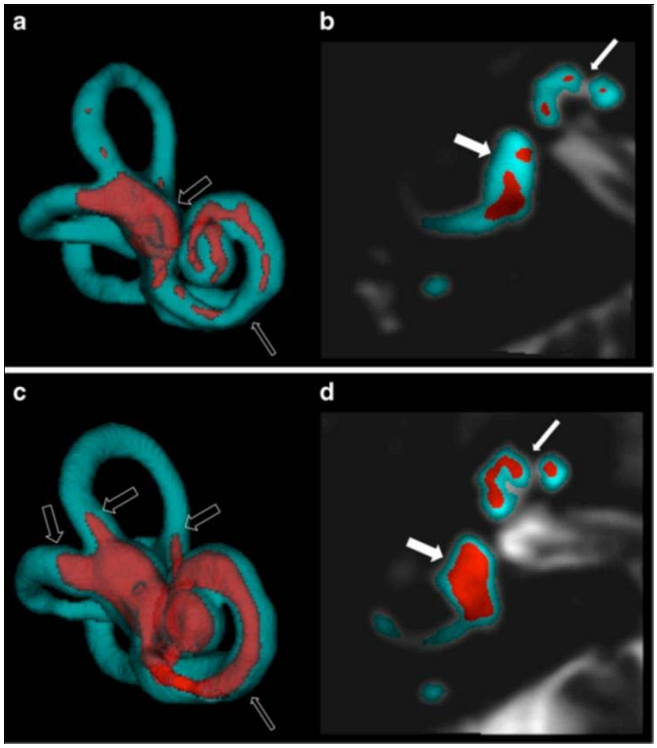

Figure 7: Computer-aided MR volumetric assessment of endolymphatic hydrops in Meniere's disease patient after intratympanic administration of Gd-DTPA. Locally Enhanced Inner ear MR Imaging (LEIM) of two patients with definite Menière's disease of the right ear after co-registration of T2-SPACE and Real-IR images and automated segmentation of total inner ear fluid space (cyan) and endolymph space (red). A and C depict the 3D reconstruction, B and D depict axial cross-sections. The three semicircular canals were continuously visualized. The interscalar septum was correctly excluded from the inner ear fluid space (thin filled arrows in B and D). A and B show the right inner ear of a patient with moderate endolymphatic hydrops. The cochlear duct could not be visualized continuously (thin transparent arrow) due to its minute dimensions. The secular and the utricularsubcompartments of the vestibulum are depicted separately (thick filled arrow) in the 2D images. C and D show the right inner ear of a patient with severe endolymphatic hydrops. The cochlear duct is markedly distended and is continuously visualized within all three cochlear turns (thin transparent arrow). The secular and the utricularsubcompartments of the vestibulum are confluent (thick filled arrow) in the 2D images. The herniation of the vestibular membraneous labyrinth into the semicircular canals is easily appreciated in the 3D images (thick transparent arrows). (*with permission to reprint the figure from EurRadiol. 2015;25: 585-595*).

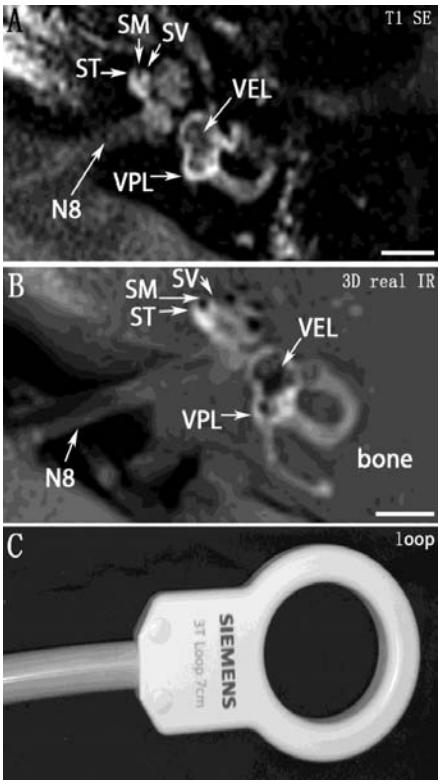

Figure 8: Demonstration of the inner ear spaces using 3 T MRI in combination with a hybridof16-ch head coil and ear coil (loop 7 cm) after intratympanic administration of Gd-DOTA. A 56-year-old man with Meniere's disease in the left ear. An endolymphatic shunt operation was performed 26 years previously. Thereafter, he was symptom free but had sudden hearing loss, tinnitus, and one vertigo attack 3 months previously. Pressure and hyperacusis remained. Initial hearing loss of 50 dB was recovered and, at the time of imaging, was 20 dB HL. The images were acquired at 24 h after transtympanic injection of 100 mMGd-DOTA using either T1-weighted Spin Echo (T1 SE) (A) or 3D inversion-recovery turbo spin echo with real reconstruction (3D real IR) (B). An additional loop coil was utilized (C). N8: 8th cranial Nerve; SM: Scala Media; ST: Scala Tympani; SV: Scalavestibuli; VEL: Vestibular Endolymph; VPL: Vestibular Perilymph. Scale bar = 5 mm.

T2-weighted 3D "Sampling Perfection with Application-optimized Contrasts using different flip angle Evolutions" (SPACE) turbo spin echo sequence (T2-SPACE) to clearly demarcate between the inner ear fluid space and bone and 3D Real-IR TSE to separate the endolymphatic spaces from the perilymphatic spaces [53]. The method involves resampling and co-registration of the T2-SPACE volume to the Real-IR volume, Contrast Limited Adaptive Histogramm Equalization (CLAHE), segmentation of the inner ear total fluid space using Random Forest Classification machine learning, fusion of this template with the 3D Real-IR image, endolymph/perilymph segmentation using a Niblack local threshold algorithm, and 3D reconstruction and volumetric quantification of EH. Involvement of computer-aided assessment minimized the artifacts created by the previous manual procedures. However, the volumetric method does not by itself allow the establishment of a diagnosis of MD in an individual patient. It is also a challenge for the imaging technician to master the complete method.

Impact of MRI coil on the image quality

For the inner ear, which has a small region of interest and low signal intensity in general, the sensitivity and pixel resolution of MRI are critical factors in meeting clinical requirements. In our experience with inner ear imaging, maximally, a 32-channel coil has been applied for data acquisition, and an 8-channel coil was tried as well. Regardless of the 3 T machine model and imaging sequences, the coils with a higher number of elements produced images with higher spatial resolution. The best image quality was achieved in the inner ear when a hybrid of16-ch head coil and ear coil (loop 7 cm) was used (Figure 8). The combinations of scanners and coils are shown in Table 2.

The sensitivity of MRI is dependent on the type of radiofrequency coil used for signal reception. By simultaneously acquiring and subsequently combining data from a multitude of closely positioned NMR receiving coils, an approach conceptually similar to phased array radar and ultrasound was developed and hence was called the "NMR phased array". The Signal-to-Noise Ratio (SNR) and resolution of a small surface coil over Fields-Of-View (FOV) were significantly improved without increasing the imaging time. Therefore, the array coils are more sensitive than the birdcage coils [54]. It is known that the higher the number of coil elements used, the higher the SNR and spatial resolution in the area located close to the coil elements. Maximally, a 96-channel receive-only coil was reported to be superior to the commercial 32-channel coil with respect to the SNR and g-factor [55]. However, increasing the number of array channels places an increased computational burden on the image reconstruction computer and substantially increases reconstruction times, especially for accelerated imaging.

Table 2: Combinations of scanners and coils that have been utilized in inner ear MRI for the detection of EH.

Scanner/company	Coil model/channel	Image quality	Hospital
Verio/Siemens	12-ch	4	Grosshadern Medical Centre, University of Munich, Germany
Verio/Siemens	32-ch head coil	4	Grosshadern Medical Centre, University of Munich, Germany
Trio/Siemens	receive-only 12-ch phased-array coil	4	Nagoya University Graduate School of Medicine, Japan
Verio/Siemens	32-ch head coil	4	Nagoya University Graduate School of Medicine, Japan
Trio-Tim /Siemens	16-ch head coil + loop ear coil	5	Tampere University Hospital, Finland
Skyra/Siemens	Tim 4G Head/Neck 20 coil	4	Changhai Hospital, Second Military Medical University, China
Verio/Siemens	32-chphased array head coil	4	Affiliated Sixth People's Hospital of Shanghai Jiao Tong University

Image quality level: 5, very good demonstration of the cochlear scalae and vestibular structures; 4, the cochlear scalae and vestibular structures were differentiated; 3, the endolymphatic and perilymphatic compartments in the cochlea and vestibule were almost differentiated; 2; the endolymphatic and perilymphatic compartments in the cochlea and vestibule were not differentiated, but the cochlear and vestibular structures were demonstrated; 1, the cochlear and vestibular structures were not demonstrated.

The superb image quality achieved in the inner ear using ahybridof16-ch head coil and ear coil (loop 7 cm) might be explained as follows. Small coils are superior for spatial resolution, but the superiority is lost in deeper tissues, such as the inner ear. Thus, a high number of coils (= also smaller coils) does not provide an advantage in this case. The detection depth is directly related to the coil diameter. The special ear coil is closer and more ideally placed to measure the inner ear than any of the coils in the head coil. Additionally, it has a larger diameter and can thus detect the signal from the deeper tissues, such as the inner ear, with a better SNR than the head coils.

Conclusion

Visualizing EH in MD patients using gadolinium-enhanced inner ear MRI is feasible in the clinic, and intratympanic administration of GdC has the advantage of introducing greater uptake of the contrast agent in the inner ear with minimal dosage over an intravenous injection. The tympanic medial wall administration of contrast agent is a minimally invasive method and has the potential for clinical applications by increasing the delivery efficacy and patient acceptance. MEMRI may be utilized to visualize calcium metabolic changes in the inner ear of MD patients. Sophisticated imaging sequences improved the sensitivity and image quality of inner ear MRI and promoted the feasibility of routine intravenous injection of GdC in clinical applications. The type of radiofrequency coil used for signal reception has a significant impact on sensitivity and image quality, and a hybrid of16-ch head coil and ear coil (loop 7 cm) is a cost-effective strategy.

Acknowledgement

The work was supported by the EC FP7 collaborative project NANOCI (grant agreement number: 281056) and the National Natural Science Foundation of China (grant number: 81170914/H1304).

References

1. Yamakawa K. Hearing organ of a patient who showed Meniere's symptoms (in Japanese). J Otolaryngol Soc Jpn. 1938; 44: 302-305.
2. Hallpike CS, Cairns H. Observations on the Pathology of Ménière's Syndrome: (Section of Otology). Proc R Soc Med. 1938; 31: 1317-1336.
3. Prosper M. Mémoire sur des lesions de l'oreille interne donnant lieu à des symptômes de congestion cérébrale apoplectiforme. Gaz Méd Paris. 1861; 16: 597-601.
4. Committee on Hearing and Equilibrium guidelines for the diagnosis and evaluation of therapy in Menière's disease. American Academy of Otolaryngology-Head and Neck Foundation, Inc. Otolaryngol Head Neck Surg. 1995; 113: 181-185.
5. Zou J, Pyykkö I, Bjelke B, Bretlau P, Tayamaga T. Endolympahtic hydrops is caused by increased porosity of stria vascularis? Barany Society Meeting; Uppsala, Sweden. 2000.
6. Zou J, Pyykkö I, Bretlau P, Klason T, Bjelke B. *In vivo* visualization of endolymphatic hydrops in guinea pigs: magnetic resonance imaging evaluation at 4.7 tesla. Ann Otol Rhinol Laryngol. 2003; 112: 1059-1065.
7. Tervahartiala P, Kivisaari L, Kivisaari R, Virtanen I, Standertskjöld-Nordenstam CG. Contrast media-induced renal tubular vacuolization. A light and electron microscopic study on rat kidneys. Invest Radiol. 1991; 26: 882-887.
8. Thomsen HS. Gadolinium-based contrast media may be nephrotoxic even at approved doses. Eur Radiol. 2004; 14: 1654-1656.
9. Thakral C, Alhariri J, Abraham JL. Long-term retention of gadolinium in tissues from nephrogenic systemic fibrosis patient after multiple gadolinium-enhanced MRI scans: case report and implications. Contrast Media Mol Imaging. 2007; 2: 199-205.
10. Zou J, Pyykkö I, Bjelke B, Dastidar P, Toppila E. Communication between the perilymphatic scalae and spiral ligament visualized by *in vivo* MRI. Audiol Neurootol. 2005; 10: 145-152.
11. Nakashima T, Naganawa S, Sugiura M, Teranishi M, Sone M, Hayashi H, et al. Visualization of endolymphatic hydrops in patients with Meniere's disease. Laryngoscope. 2007; 117: 415-420.
12. Kimura RS. Experimental blockage of the endolymphatic duct and sac and its effect on the inner ear of the guinea pig. A study on endolymphatic hydrops. Ann Otol Rhinol Laryngol. 1967; 76: 664-687.
13. Tomiyama S. Development of endolymphatic hydrops following immune response in the endolymphatic sac of the guinea pig. Acta Otolaryngol. 1992; 112: 470-478.
14. Tomiyama S, Kinoshita T, Jinnouchi K, Ikezono T, Gotoh Y, Pawanker R, et al. Fluctuating hearing loss following immune reaction in the endolymphatic sac of guinea pigs. ORL J Otorhinolaryngol Relat Spec. 1995; 57: 122-128.
15. Kumagami H. Endolymphatic hydrops induced by noise exposure. Auris Nasus Larynx. 1992; 19: 95-104.
16. Hughes GB, Barna BP, Kinney SE, Calabrese LH, Nalepa NJ. Clinical diagnosis of immune inner-ear disease. Laryngoscope. 1988; 98: 251-253.
17. Suzuki M, Kitahara M. Immunologic abnormality in Menière's disease. Otolaryngol Head Neck Surg. 1992; 107: 57-62.
18. Zou J. [A preliminary study on the mechanism of immune injury of Menière's disease--type V collagen play the role of antigen]. Zhonghua Er Bi Yan Hou Ke Za Zhi. 1992; 27: 14-16, 60.
19. Baron F, Legent F, Collet M. [Sudden deafness. A case of Meniere-type vertigo secondary to exposure to a very loud noise and treated by section of the vestibular nerve, and a case of spontaneous perilymphatic fistula]. Ann Otolaryngol Chir Cervicofac. 1973; 90: 427-436.
20. Ylikoski J. Delayed endolymphatic hydrops syndrome after heavy exposure to impulse noise. Am J Otol. 1988; 9: 282-285.
21. Pyykkö I, Zou J, Poe D, Nakashima T, Naganawa S. Magnetic resonance imaging of the inner ear in Meniere's disease. Otolaryngol Clin North Am. 2010; 43: 1059-1080.
22. Zou J, Pyykkö I, Bjelke B, Esko Toppila. *In vivo* MRI visualization of endolymphatic hydrops induced by keyhole limpet hemocyanin round window immunization. Audiological Medicine. 2007; 5: 182-187.
23. Paparella MM, de Sousa LC, Mancini F. Meniere's syndrome and otitis media. Laryngoscope. 1983; 93: 1408-1415.
24. Counter SA, Bjelke B, Borg E, Klason T, Chen Z, Duan ML. Magnetic resonance imaging of the membranous labyrinth during *in vivo* gadolinium (Gd-DTPA-BMA) uptake in the normal and lesioned cochlea. Neuroreport. 2000; 11: 3979-3983.
25. Duan M, Bjelke B, Fridberger A, Counter SA, Klason T, Skjönsberg A, et al. Imaging of the guinea pig cochlea following round window gadolinium application. Neuroreport. 2004; 15: 1927-1930.
26. Zou J, Yoshida T, Ramadan UA, Pyykkö I. Dynamic enhancement of the rat inner ear after ultra-small-volume administration of Gd-DOTA to the medial wall of the middle ear cavity. ORL J Otorhinolaryngol Relat Spec. 2011; 73: 275-281.
27. Zou J, Peng R, Zheng G, Zhang Q, Toppila E, Zheng H, et al. Improvement in the inner ear symptoms of patients with Meniere's disease after treatment using low-frequency vibration: A preliminary report. Edorium J Otolaryngology. 2015; 2: 5-13.
28. Zou J, Poe D, Ramadan UA, Pyykkö I. Oval window transport of Gd-dOTA from rat middle ear to vestibulum and scala vestibuli visualized by *in vivo* magnetic resonance imaging. Ann Otol Rhinol Laryngol. 2012; 121: 119-128.
29. Zou J, Pyykkö I. Enhanced oval window and blocked round window passages for middle-inner ear transportation of gadolinium in guinea pigs with a

perforated round window membrane. Eur Arch Otorhinolaryngol. 2015; 272: 303-309.

30. Shi H, Li Y, Yin S, Zou J. The predominant vestibular uptake of gadolinium through the oval window pathway is compromised by endolymphatic hydrops in Ménière's disease. Otol Neurotol. 2014; 35: 315-322.

31. Kakigi A, Nishimura M, Takeda T, Okada T, Murata Y, Ogawa Y. Effects of gadolinium injected into the middle ear on the stria vascularis. Acta Otolaryngol. 2008; 128: 841-845.

32. Louza JP, Flatz W, Krause E, Gürkov R. Short-term audiologic effect of intratympanic gadolinium contrast agent application in patients with Ménière's disease. Am J Otolaryngol. 2012; 33: 533-537.

33. Louza J, Krause E, Gürkov R. Hearing function after intratympanic application of gadolinium-based contrast agent: A long-term evaluation. Laryngoscope. 2015.

34. Pautler RG, Silva AC, Koretsky AP. *In vivo* neuronal tract tracing using manganese-enhanced magnetic resonance imaging. Magnetic resonance in medicine: official journal of the Society of Magnetic Resonance in Medicine / Society of Magnetic Resonance in Medicine. 1998; 40: 740-748.

35. Dryselius S, Grapengiesser E, Hellman B, Gylfe E. Voltage-dependent entry and generation of slow Ca2+ oscillations in glucose-stimulated pancreatic beta-cells. Am J Physiol. 1999; 276: E512-518.

36. Mori Y, Amano T, Sasa M, Yajin K. Cytochemical and patch-clamp studies of calcium influx through voltage-dependent Ca2+ channels in vestibular supporting cells of guinea pigs. European archives of oto-rhino-laryngology: official journal of the European Federation of Oto-Rhino-Laryngological Societies. 1998; 255: 235-239.

37. Imon K, Amano T, Ishihara K, Sasa M, Yajin K. Existence of voltage-dependent Ca2+ channels in vestibular dark cells: cytochemical and whole-cell patch-clamp studies. European archives of oto-rhino-laryngology: official journal of the European Federation of Oto-Rhino-Laryngological Societies. 1997; 254: 287-291.

38. Watanabe T, Frahm J, Michaelis T. Manganese-enhanced MRI of the mouse auditory pathway. Magn Reson Med. 2008; 60: 210-212.

39. Lee JW, Park JA, Lee JJ, Bae SJ, Lee SH, Jung JC, et al. Manganese-enhanced auditory tract-tracing MRI with cochlear injection. Magn Reson Imaging. 2007; 25: 652-656.

40. Jin SU, Lee JJ, Hong KS, Han M, Park JW, Lee HJ, et al. Intratympanic manganese administration revealed sound intensity and frequency dependent functional activity in rat auditory pathway. Magnetic resonance imaging. 2013; 31: 1143-1149.

41. Yu X, Wadghiri YZ, Sanes DH, Turnbull DH. *In vivo* auditory brain mapping in mice with Mn-enhanced MRI. Nat Neurosci. 2005; 8: 961-968.

42. Holt AG, Bissig D, Mirza N, Rajah G, Berkowitz B. Evidence of key tinnitus-related brain regions documented by a unique combination of manganese-enhanced MRI and acoustic startle reflex testing. PLoS One. 2010; 5: e14260.

43. Gröschel M, Müller S, Götze R, Ernst A, Basta D. The possible impact of noise-induced Ca2+-dependent activity in the central auditory pathway: a manganese-enhanced MRI study. Neuroimage. 2011; 57: 190-197.

44. Gröschel M, Hubert N, Müller S, Ernst A, Basta D. Age-dependent changes of calcium related activity in the central auditory pathway. Exp Gerontol. 2014; 58: 235-243.

45. Andrews M, Giger ML, Roman BB. Manganese-enhanced MRI detection of impaired calcium regulation in a mouse model of cardiac hypertrophy. NMR Biomed. 2015; 28: 255-263.

46. Zou J, Pyykkö I. Calcium Metabolism Profile in Rat Inner Ear Indicated by MRI After Tympanic Medial Wall Administration of Manganese Chloride. Ann Otol Rhinol Laryngol. 2015; Jul 29. pii: 0003489415597916. [Epub ahead of print].

47. Naganawa S, Satake H, Kawamura M, Fukatsu H, Sone M, Nakashima T. Separate visualization of endolymphatic space, perilymphatic space and bone by a single pulse sequence; 3D-inversion recovery imaging utilizing real reconstruction after intratympanic Gd-DTPA administration at 3 Tesla. Eur Radiol. 2008; 18: 920-924.

48. Naganawa S, Kawai H, Sone M, Nakashima T. Increased sensitivity to low concentration gadolinium contrast by optimized heavily T2-weighted 3D-FLAIR to visualize endolymphatic space. Magn Reson Med Sci. 2010; 9: 73-80.

49. Naganawa S, Yamazaki M, Kawai H, Bokura K, Sone M, Nakashima T. Visualization of endolymphatic hydrops in Meniere's disease with single-dose intravenous gadolinium-based contrast media using heavily T(2)-weighted 3D-FLAIR. Magnetic resonance in medical sciences: MRMS: an official journal of Japan Society of Magnetic Resonance in Medicine. 2010; 9: 237-242.

50. Naganawa S, Yamazaki M, Kawai H, Bokura K, Sone M, Nakashima T. Imaging of Ménière's disease after intravenous administration of single-dose gadodiamide: utility of subtraction images with different inversion time. Magn Reson Med Sci. 2012; 11: 213-219.

51. Naganawa S, Yamazaki M, Kawai H, Bokura K, Sone M, Nakashima T. Imaging of Ménière's disease after intravenous administration of single-dose gadodiamide: utility of multiplication of MR cisternography and HYDROPS image. Magn Reson Med Sci. 2013 25;12 (1):63-8.

52. Naganawa S, Yamazaki M, Kawai H, Bokura K, Iida T, Sone M, Nakashima T. MR imaging of Ménière's disease after combined intratympanic and intravenous injection of gadolinium using HYDROPS2. Magn Reson Med Sci. 2014;13 (2):133-7.

53. Gürkov R, Berman A, Dietrich O, Flatz W, Jerin C, Krause E, et al. MR volumetric assessment of endolymphatic hydrops. Eur Radiol. 2015; 25: 585-595.

54. Roemer PB, Edelstein WA, Hayes CE, Souza SP, Mueller OM. The NMR phased array. Magn Reson Med. 1990; 16: 192-225.

55. Wiggins GC, Polimeni JR, Potthast A, Schmitt M, Alagappan V, Wald LL. 96-Channel receive-only head coil for 3 Tesla: design optimization and evaluation. Magn Reson Med. 2009; 62: 754-762.

Austin J Radiol - Volume 2 Issue 6 - 2015
ISSN : 2473-0637 | www.austinpublishinggroup.com

Citation: Zou J, Pyykkö I, Yoshida T, Gürkov R, Shi H, Li Y, et al. Milestone Research on Meniere's Disease by Visualizing Endolymphatic Hydrops Using Gadolinium-Enhanced Inner Ear MRI and the Challenges in Clinical Applications. Austin J Radiol. 2015; 2(6): 1035.